

Lopsidedness in Early Type Disk Galaxies

Gregory Rudnick, Hans-Walter Rix¹
Steward Observatory, The University of Arizona

ABSTRACT

We quantify the mean asymmetry of 54 face-on, early type disk galaxies (S0 to Sab) using the amplitude of the $m = 1$ azimuthal Fourier component of the R-band surface brightness. We find that the median lopsidedness, $\langle A_1/A_0 \rangle$, of our sample is 0.11 and that the most lopsided 20% of our galaxies have $\langle A_1/A_0 \rangle \geq 0.19$. Asymmetries in early type disks appear to be of similar frequency and strength as in late type disk galaxies (Zaritsky and Rix 1997.) We have observed our early type disks in a bandpass (R-Band) in which the light is dominated by stars with ages greater than 10^9 yrs, and therefore are seeing azimuthal asymmetries in the stellar *mass* distribution. The similar degree of lopsidedness seen in disks of very different star formation rates indicates that the lopsidedness in all galactic disks is primarily due to azimuthal mass asymmetries. Hence, 20% of all disk galaxies (regardless of Hubble Type) have azimuthal asymmetries, $\langle A_1/A_0 \rangle \geq 0.19$, in their stellar disk mass distribution, confirming lopsidedness as a dynamical phenomenon.

Subject headings: galaxies: kinematics and dynamics — galaxies: photometry — galaxies: spiral — galaxies: structure

1. Introduction

Just as a human face may mirror traumatic events in its past, so may a galaxy's structure reflect its dynamical history. In this paper we explore one potential probe of the dynamical past of disk galaxies, their *lopsidedness*. In the context of this paper, lopsidedness is defined as a significant bulk asymmetry in the stellar mass distribution of a galactic disk. For nearly face-on galaxies, these asymmetries manifest themselves observationally as a shifting of the outer isophotes of the stellar light.

¹Alfred P. Sloan Fellow

Baldwin et al. (1980) were the first to point out that the HI profiles of spiral galaxies are frequently lopsided, and suggested that this lopsidedness may stem from weak interactions in the galaxy’s past, or from lopsided orbits. Richter and Sancisi (1994) using a much larger galaxy sample to study the frequency of lopsidedness, concluded that over 50% of all disk galaxies had significant asymmetries in their HI profiles. These HI asymmetries are present both in the projected flux distributions and in velocity space.

A systematic attempt to examine the frequency of asymmetries in the stellar light of galaxies has been made by Rix and Zaritsky, 1995 and Zaritsky and Rix, 1997 (hereafter RZ95 and ZR97) and a recent optical study of symmetry in nearby disk galaxies has been carried out by Conselice (1998.) Using near-IR photometry of face-on galaxies, ZR97 found that about one fifth of all late type spiral galaxies exhibited significant lopsidedness. They defined lopsidedness via the amplitude of the $m = 1$ Fourier component of the azimuthal decomposition of the galaxy’s surface brightness. It is possible to construct self-consistent asymmetric disk models (Syer and Tremaine, 1996) and some N-body work has shown that lopsided instabilities may occur in the presence of retrograde orbits (Zang and Hohl, 1978; Sellwood and Merritt, 1994) or in the absence of a massive halo (Sellwood, 1985). These authors also find that co-rotating galaxies with massive halos are stable against intrinsic $m = 1$ instabilities.

Since intrinsic disk instabilities in spirals appear not to be the dominant cause of lopsidedness, external potential perturbations are the most plausible candidate mechanism. N-body simulations (Walker et al. 1996; ZR97) have shown that the merger of a small galaxy with a large disk galaxy can produce the type and degree of asymmetries found in RZ95 and ZR97, if their mass ratio is $\sim 1/10$. Recent N-body work by Levine and Sparke (1998) shows that lopsided modes may persist in disk galaxies if the disks are off-center with respect to a massive host halo with a large, flat core. They propose that a galaxy may become lopsided if it accretes enough matter to push it away from the center of the halo. It stands to reason that these asymmetries may also be produced by weak, non-cataclysmic encounters with other galaxies (Barnes, Hernquist 1992 and references therein.) Lifetimes of these asymmetries can be estimated from phase mixing (Baldwin et al. 1980; RZ95) or through analysis of N-Body simulations (Walker et al. 1996; ZR97); both estimates point to lifetimes of 5-10 rotation periods, or $1 \sim \text{Gyr}$.

For interpreting lopsidedness it is crucial to know whether the observable asymmetries in the stellar *light* reflect asymmetries in the stellar *mass*. Late type disk galaxies (such as those used in RZ95 and ZR97) with relatively high star formation rates contain many young, bright stars. As we will show later, in Sbc galaxies, up to 25% of the light in the light in the R-Band can come from stars younger than 0.1 Gyrs (OB stars.) An asymmetric distribution

of such a luminous, young population could result in a high observed asymmetry, even if the underlying mass structure were in fact close to symmetric. To avoid this potential pitfall, we assembled a sample of disk galaxies with low star formation rates, those limited to Hubble Types from S0 to Sab (Kennicutt et al. 1994), with the aim of comparing the incidence of lopsidedness in this new sample to that in RZ95,ZR97. If significant asymmetries are similarly frequent, we may conclude that they are in fact dynamical in origin and are not merely azimuthal variations in the mass-to-light ratios within the galaxies.

The layout of the paper is as follows. In §2 we will discuss the sample selection, observations and reduction techniques; In §3 we will describe the data analysis methods. The results, including the frequency of lopsidedness, are presented and discussed in §4. In §5 we will present our conclusions as well as the directions for future follow-up work.

2. The Data

2.1. Sample Selection & Observations

Our sample is comprised of 60 galaxies taken from the RC3 catalogue (De Vaucouleurs, 1991), selected according to the following criteria: $m_B \leq 14$, $cz \leq 10,000$ km/s, $b/a \leq 0.65$ ($49^\circ \leq i \leq 0^\circ$), $0 \leq T \leq 2$, and a maximum diameter of $4'$. The median diameter of the galaxies on our sample was $2.3'$. The magnitude and redshift limits were chosen to minimize the required exposure times, while the axis ratio of the galaxies was constrained to reduce projection effects in our analysis. For reasons explained in §3.2, only 54 of these galaxies were included in our final sample (see Table 1.)

The galaxies were observed on three runs at the 2.3-meter Bok reflector on Kitt Peak (April 15-17th, 1996) and at the 1.5-meter reflector on Mt. Bigelow (November 10-13th, 1996 and April 9-14th, 1997). For these three runs, the CCD pixel scales were $0.3''/\text{pix}$, $0.9''/\text{pix}$ and $0.4''/\text{pix}$, respectively, with fields-of-view of $3' \times 2'$, $9.8' \times 9.3'$ and $3.3' \times 3.3'$. The median seeing at the 2.3-meter was $1.5''$ while the median seeing during the November and April runs on the 60-inch were $1.7''$ and $1.4''$ respectively.

A Nearly-Mould R-band filter ($\lambda_{center} = 650nm$) was used at the 2.3-meter. The filters used for the November and April 60-inch runs were respectively a Mould R-band filter with $\lambda_{center} = 650nm$ and a Kron-Cousins R-band filter with $\lambda_{center} = 650nm$.

In order to emphasize the light coming from stellar populations that trace the stellar mass distribution (old stars), observations were previously carried out in the near-IR (K and I bands, RZ95; ZR97.) In this paper we study galaxies with lower star formation

rates; where we can expect the R-band light to be a sufficient tracer of phase-mixed stellar populations. Using simple models (see RZ95, Appendix B) for the star formation history of Sa galaxies (Kennicutt et al. 1994) we determined that the light from stars younger than 10^8 years ($t \leq t_{orbit}$) typically contributes only 4% to the total light in the R-Band, while stars younger than 10^9 ($t \leq 10t_{orbit}$) years contribute 12% of the total R-Band light. Going to longer wavelengths (e.g. I) would slightly decrease the contribution from younger stars but this gain is not worth the increased observing expense. In contrast, a galaxy with the star formation history of a stereotypical Sbc (Kennicutt et al. 1994), would lead to 24% of the R-Band light originating from stars younger than 10^8 years and 50% from stars younger than 10^9 years.

2.2. Reduction

The initial image reduction was carried out with standard IRAF [†] routines. The 2.3-meter images were flat-fielded with a combination of dome flats and twilight flats; the 1.5-meter images were flattened with twilight and smoothed night sky flats. For the 2.3-meter images, the dome flats were used to remove the small scale variations, while the sky flats (smoothed) were used to remove the large scale variations. At the 1.5-meter the smoothed night sky and twilight images were all combined into one flat which accounted for both the small and large scale variations. The quality of the large-scale flat-fielding was estimated from the variance of the median sky level at the four corners of the images. The large diameter of the galaxies compared to the field of view at the 2.3-meter, precluded such an estimate in many cases. Whenever the flat-field quality could be checked however, it was found to be 1 – 2%. At the 1.5-meter, the larger field of view allowed a more accurate determination of the flat-field quality and the images typically were flattened to within 0.5%. The superior flat-field quality of the 1.5-meter data may be due to the high S/N night sky flats.

Point sources in the images were selected using *daofind* and surrounding pixels were excised in the subsequent analysis to a radius where the stellar point spread function brightness had declined to the level of the sky.

3. Data Analysis

[†]IRAF is distributed by the National Optical Astronomical Observatories, which are operated by AURA, Inc. under contract to the NSF.

3.1. Fourier Decomposition

There is no unique measure of asymmetry in galaxies. Here, we use an approach that provides information not only about the magnitude of the disk asymmetry, but also about its angular phase and its radial dependence. Although we only analyze the radial dependence of the asymmetry, we use the angular dependence in our visual verification of lopsided structure. Fourier decomposition in polar coordinates has been employed previously (RZ95 and ZR97 and references therein), and we will not describe it in detail. Briefly, we center a polar coordinate grid on the galaxy nucleus, with 16 azimuthal and 45 radial bins that extend logarithmically from 2.5 to 180 pixels. For our April, 1996 run at the 2.3-meter and our November, 1996 and April, 1997 runs at the 1.5-meter, this radial outer limit corresponds respectively to 0.9', 2.7' and 1.2'. By these limits, our S/N had already declined below the level required to perform a successful determination of lopsidedness. The nucleus is identified with the brightest point in a galaxy's center; slight deviations from this do not affect significantly the subsequent analysis of asymmetries in the outer parts (RZ95.)

Specifically, we decompose the image intensity in an annulus of mean radius R_m into the form:

$$I(R_m, \phi) = a_o \times \left(1 + \sum_{j=1}^N a_j e^{-i[j(\phi_j - \phi_j^o)]} \right) \quad (1)$$

Where for each radius, $|a_o|(R)$ is the average luminosity, $|a_1|(R)$ describes the lopsidedness and $|a_2|(R)$ is the bisymmetric fluctuation amplitude (arising from ellipticity, projection effects, etc.) Likewise, ϕ_j^o is the position angle of each component a_j . Although asymmetries may put power into any odd a_j , most of the power is usually concentrated in the a_1 term (RZ95.) We define the luminosity normalized quantities $A_j \equiv a_j/a_o$.

In addition to the Fourier decomposition, we fit a bulge-disk profile to the galaxy images (using a $R^{1/4}$ bulge and exponential disk law.) We calculate the mean asymmetry, $\langle A_1 \rangle$, for each galaxy by taking the radial average of the asymmetry from 1.5 to 2.5 disk scale lengths weighted by the errors as described in §3.1. The radial limits encompass 26% of the disk light and straddle the half light radius of the disk. Averaging over a range in radii reduces the effect of isolated asymmetric peaks on our analysis and also gives us a global measure of the lopsidedness for each galaxy in our sample.

Because the A_j 's are positive definite in the presence of errors $\Delta \tilde{A}_1$, the expectation value of the A_1 measurement will be higher than the true value \tilde{A}_1 . The measured value at each radius is given by $A_1^2 = \tilde{A}_1^2 + \Delta A_1^2$. In ZR97, this correction was not included in their determination of $\langle A_1 \rangle$. We have examined the effect that this omission will have on our comparison with ZR97, and it was found that the difference between $\langle \tilde{A}_1 \rangle$ and $\langle A_1 \rangle$ in our sample is about 1%. Therefore, our choice to use $\langle \tilde{A}_1 \rangle$ instead of $\langle A_1 \rangle$ will not effect our

comparison.

3.2. Radial Dependence of the Asymmetries

In Fig. 1, we plot the median $\tilde{A}_1(L(\leq R)/L(tot))$ profiles of the most lopsided 20% of our galaxies and the least lopsided 80% of our galaxies with $R_{max} \geq 2.5R_{exp}$ ($L(\leq R)/L(tot) \geq 0.71$.) The centers of almost all the galaxies are very symmetric regardless of the asymmetry in their outer parts. Therefore using the inner portions of galaxies ($L(\leq R)/L(tot) \leq 0.2$) will not aid us in determining the $\langle \tilde{A}_1 \rangle$ of the bulk disk. The outer radial limit of $2.5R/R_{exp}$ was chosen due to S/N constraints.

The decrease in the value of $\tilde{A}_1(L(\leq R)/L(tot))_{lopsided}$ for $L(\leq R)/L(tot) \geq 0.71$ ($R/R_{exp} \geq 2.5$) is due to the fact that two of our more lopsided galaxies only have measurements out to $R \approx 2.5R_{exp}$. Because we are missing two highly lopsided galaxies for $R \geq 2.5R_{exp}$, the median lopsidedness of the sample drops at these radii. Note, that if most of the asymmetric galaxies were classified as being lopsided because of isolated peaks at some random radius, $1.5R_{exp} \leq R \leq 2.5R_{exp}$, in their $\tilde{A}_1(R)$ profiles, the two median plots would look very similar.

Examining the position angle of the asymmetries, we find that there is very little variation with radius. This implies that lopsidedness cannot be attributed to the existence of a wound one-armed spiral.

3.3. Errors

The analysis program (RZ95,ZR97) uses Poisson statistics and the quality of the flat-field to determine the error in $A_1(R)$. Beyond $R \approx R_{exp}$, the errors in measuring $A_1(R)$ are dominated by the quality of the flat-fielding, δI_{counts} . We extended our measurements radially until the flux of the galaxy dropped to three times the flat-field error, $I_{galaxy} = 3 \times \delta I$. For an average sky surface brightness, $\mu_{sky} = 21.5mag/asec^2$ and an average flat-field quality, $\delta I/I_{sky} = 1\%$, our typical limiting surface brightness was $\mu_{galaxy} = 25.3mag/asec^2$. An underestimate of the flat-field errors will lead to spurious asymmetries in the galaxy's outer regions. To explore this potential problem, we examined all galaxies which showed significant lopsidedness in their outer regions and verified both that the indicated lopsidedness had a visible counterpart, and that the flat field quality was correctly determined. None of our measurements of significant lopsidedness were found to be caused by these flat-field errors.

By re-analyzing the images with a coarse binning of 25 radial and 10 azimuthal bins, we found that the R_{exp} and $\langle \tilde{A}_1 \rangle$ estimates depend only negligibly on the grid parameters.

The analysis of images taken on consecutive nights with identical instruments was found with few exceptions to show excellent agreement. In a few cases, the images taken at different telescopes with differing instruments exhibited disagreement. In all but one of these cases (NGC 4580), the discrepancies in $\langle \tilde{A}_1 \rangle$ were accounted for by the known errors and usually resulted from differing values for the fitted disk scale lengths, or from slight variations in the $A_1(R)$ profiles. Only for NGC 4580, were we unable to account for the differences and so discarded it from the sample.

Further, 6 of the 60 objects imaged (not including NGC 4580) were eliminated because their radial measurements did not extend to $R \geq 2.5R_{exp}$.

In the end, the error $\Delta \langle \tilde{A}_1 \rangle$ for each image is comprised of three different elements added in quadrature, i) the statistical error of the mean ii) the variance of the distribution as measured between 1.5 and $2.5R_{exp}$ iii) the systematic error (0.035) derived by taking the average difference in $\langle \tilde{A}_1 \rangle$ between multiple images of the same objects.

4. Results and Discussion

4.1. Wavelength Dependence of Lopsidedness

To illustrate the wavelength dependence of lopsidedness, we obtained UBVRI images of 3 late type disk galaxies, known to be quite asymmetric in the near-IR from ZR97; the characteristics for these galaxies are given in Table 2.

As is shown in Fig. 2, the wavelength of the observation does affect the measured lopsidedness, with I-Band measurements giving the lowest values of $\tilde{A}_1(R)$. This is consistent with the prediction of stellar population models that much of the U (and B) light may come from very young, and hence not yet phase mixed, stars. Because the V,R and I-bands all have very similar $\tilde{A}_1(R)$ profiles, we can assume that the V and R-bands both sample the mass distribution with comparable accuracy as I. This implies that our method loses no reliability by going to shorter wavelengths than those used by ZR97.

4.1.1. *Is Lopsidedness Caused by Dust*

In highly inclined disk galaxies, dust can dim the near side of the galaxy more than the far side, leading to a non-zero $m=1$ amplitude. Using plausible estimates for the optical depth of an SO/Sa/Sab galaxy ($0.5 \leq \tau_V(\text{face-on}) \leq 1.0$), the magnitude of such an asymmetry in our face-on sample ($\langle i \rangle = 37^\circ$) is at most $\sim 3\%$ (Byun et al., 1994.) Such global dust asymmetries would manifest themselves as a correlation between the inclination angle and the frequency of lopsidedness. A K-S test shows that the distribution of lopsidedness among the most inclined third of our sample galaxies has a 96% probability of being drawn from the same distribution as the least inclined two-thirds.

As dust produces an asymmetry along the minor axis, it should induce a correlation between ϕ_1^o and ϕ_2^o . A K-S test reveals that the cumulative distribution of $\phi_{diff} = |\langle \phi_2^o \rangle - \langle \phi_1^o \rangle|$ has a 96% chance of being drawn from a random distribution, as expected for intrinsic lopsidedness.

If dust were the primary cause of lopsidedness, the trend of decreasing asymmetry with increasing wavelength, should continue to our reddest band. As Figure 2 shows however, the asymmetry profiles for V,R and I are almost identical.

4.2. Frequency of Lopsidedness

To determine the percentage of galaxies which are “significantly” lopsided, a lopsidedness threshold must be chosen (RZ95,ZR97). Alternatively, we can simply use the cumulative distribution of $\langle \tilde{A}_1 \rangle$. This distribution is plotted in Figure 3, and shows that the majority of galaxies are quite symmetric. The median value for $\langle \tilde{A}_1 \rangle$ in our sample is 0.11. 20% of our galaxies have $\langle \tilde{A}_1 \rangle \geq 0.19$.

To compare the frequency of lopsidedness in ZR97 to that in our sample, we must understand any systematic differences in the reduction or analysis of our different data. ZR97 used a simpler approach to eliminate superimposed foreground stars causing a small artificial increase of 0.03 in the measured lopsidedness. To compensate for this, we subtracted 0.03 from the $\langle \tilde{A}_1 \rangle$ measures of ZR97. With this correction, the median $\langle \tilde{A}_1 \rangle$ in ZR97 is 0.13. Likewise, 20% of their galaxies have $\langle \tilde{A}_1 \rangle \geq 0.19$.

Typical errors in the measurement of $\langle \tilde{A}_1 \rangle$ (0.02 for ZR97 and 0.07 for our sample) are similar to the difference between the median values and between the 20% points and so the frequency of lopsidedness in our sample is indistinguishable to that of ZR97.

The most direct determination of the frequency of lopsidedness would be achieved with

a volume limited sample. In a magnitude limited sample such as ours however, there may be ambiguities because weak, tidal interactions may cause both lopsidedness, and increased star formation rates (Mihos, Hernquist 1994; Hernquist, Mihos 1995) The volume sampled by lopsided galaxies would hence be larger than that sampled by symmetric galaxies, leading us to overestimate the actual frequency. However, the link between lopsidedness and recent star formation is poorly understood and so at the present time this effect cannot be accounted for.

5. Conclusions and Future Work

We have determined the median $\langle \tilde{A}_1 \rangle$ in our sample of early type disk galaxies to be 0.11. We have also determined that 20% of the galaxies in our sample have $\langle \tilde{A}_1 \rangle \geq 0.19$. By looking in the R-band and by selecting galaxies with typically low star formation rates, we have picked a compromise between efficiency and the minimization of the contributions from young (i.e. non phase-mixed), bright stars and hence we are primarily viewing actual azimuthal variations in the stellar mass distributions of the early type disks in our sample.

By comparing the value of $\langle \tilde{A}_1 \rangle$ which is lower than that for 50% and 20% of our galaxy sample, to that measured for late type spirals by ZR97 (0.13 and 0.19 respectively), we can address the issue of whether the asymmetries seen in ZR97 are also caused by variations in the stellar mass distribution of late type disk galaxies. If asymmetric star formation were important in creating asymmetric light distributions, we would expect that late type disk galaxies would have a higher incidence of lopsidedness than early type spirals. Since this is not the case, we are led to conclude that lopsidedness in disk galaxies of all types reflects primarily variations in the stellar mass distributions. Our data then show that one-fifth of *all* disk galaxies have $\langle \tilde{A}_1 \rangle \geq 0.19$.

The volume correction discussed in section 4.2 affects our measurement of the frequency of lopsidedness and the possibility of systematic brightening of lopsided galaxies via an increased star formation rate needs to be explored in more detail. Comparison of the recent star formation history of lopsided galaxies to that of symmetric galaxies is needed to study this effect, and is also needed to help better establish a cause of lopsidedness. A study of this nature is being carried out this spring by the authors.

Further N-Body simulations also need to be carried out to determine if the types and magnitudes of asymmetries seen in our samples can be reproduced by weak interactions as well as by minor mergers. It is also necessary to better determine if isolated phenomena (e.g. instabilities) result in asymmetries similar in morphology and magnitude to those we

have measured.

Greg Rudnick and H.-W. Rix would like to thank Robert Kennicutt for valuable discussions. We would also like to thank James Pizagno for assisting with our observing program.

Table 1. Image Sample

object name	T	D ₂₅ ^a [']	v _{rec} [km/s]	b/a ^b	R _{exp} ["]	R _{max} /R _{exp}	⟨ \tilde{A}_1 ⟩
<i>IC</i> 520	2.0	1.95	3528	0.79	13.0	2.95	0.088 ± .126
<i>NGC</i> 0023	1.0	2.09	4635	0.64	14.0	2.93	0.049 ± 0.039
<i>NGC</i> 0828	1.0	2.88	5181	0.77	15.5	4.68	0.12 ± 0.045
<i>NGC</i> 2342	0.0	1.38	5209	0.93	14.6	2.62	0.56 ± 0.066
<i>NGC</i> 2460	1.0	2.45	1442	0.76	7.4	4.72	0.045 ± 0.038
<i>NGC</i> 2551	0.2	1.66	2263	0.67	12.0	4.25	0.063 ± 0.069
<i>NGC</i> 2554 ^c	0.0	1.50	4126	0.74	14.0	3.43	0.092 ± 0.032
<i>NGC</i> 2599	1.0	1.86	4690	0.89	16.5	2.87	0.124 ± 0.031
<i>NGC</i> 2681	0.0	3.63	692	0.91	32.5	2.92	0.040 ± 0.037
<i>NGC</i> 2775 ^c	2.0	1.63	1340	0.77	17.4	5.08	0.093 ± 0.026
<i>NGC</i> 2782	1.0	3.47	2562	0.74	20.4	2.87	0.19 ± 0.098
<i>NGC</i> 2855	0.0	2.45	1910	0.89	9.0	4.70	0.11 ± 0.11
<i>NGC</i> 2993 ^c	1.0	1.13	2227	0.69	9.4	4.40	0.162 ± 0.055
<i>NGC</i> 3277	2.0	1.95	1460	0.89	8.2	4.37	0.046 ± 0.048
<i>NGC</i> 3415	−0.5	2.09	3177	0.63	9.8	4.01	0.038 ± 0.037
<i>NGC</i> 3442	1.0	0.62	1724	0.76	3.5	4.11	0.286 ± 0.047
<i>NGC</i> 3504	2.0	2.69	1518	0.77	19.6	3.86	0.106 ± 0.046
<i>NGC</i> 3611	1.0	2.09	1754	0.81	12.2	3.77	0.118 ± 0.043
<i>NGC</i> 3682	0.0	1.66	1543	0.66	7.2	4.65	0.145 ± 0.060
<i>NGC</i> 3720	0.9	0.95	5958	0.91	5.4	4.38	0.122 ± 0.060
<i>NGC</i> 3732 ^c	0.0	1.09	1682	0.95	6.53	3.62	0.169 ± 0.026
<i>NGC</i> 3884	0.0	2.09	6869	0.64	13.7	3.37	0.213 ± 0.210
<i>NGC</i> 4245	0.0	2.88	890	0.76	18.2	3.42	0.026 ± 0.038
<i>NGC</i> 4277 ^c	0.0	1.02	2516	0.83	9.0	3.26	0.014 ± 0.028
<i>NGC</i> 4314	1.0	4.17	963	0.89	11.5	5.40	0.010 ± 0.035
<i>NGC</i> 4369 ^c	1.0	1.32	988	0.98	8.6	5.41	0.238 ± 0.068
<i>NGC</i> 4378	1.0	2.88	2563	0.93	12.2	3.46	0.027 ± 0.037
<i>NGC</i> 4384 ^c	1.0	1.11	2400	0.77	6.7	4.48	0.153 ± 0.040
<i>NGC</i> 4415	0.0	1.35	825	0.89	7.0	4.54	0.040 ± 0.992
<i>NGC</i> 4421	0.0	2.69	1692	0.76	17.0	3.01	0.014 ± 0.037
<i>NGC</i> 4454 ^c	0.0	1.30	2373	0.85	14.6	3.39	0.080 ± 0.038
<i>NGC</i> 4457	0.0	2.69	738	0.85	22.8	2.72	0.113 ± 0.042
<i>NGC</i> 4464	0.0	1.07	1255	0.76	5.0	4.27	0.006 ± 0.036
<i>NGC</i> 4470	1.0	1.29	2358	0.72	10.6	3.39	0.494 ± 0.075

Table 1—Continued

object name	T	D ₂₅ ^a [']	v _{rec} [km/s]	b/a ^b	R _{exp} ["]	R _{max} / R _{exp}	⟨ \tilde{A}_1 ⟩
<i>NGC</i> 4492	1.0	1.70	1772	0.93	10.4	4.01	0.115 ± 0.143
<i>NGC</i> 4566	0.0	1.26	5290	0.71	12.4	2.54	0.151 ± 0.081
<i>NGC</i> 4643	0.0	3.09	1399	0.74	4.9	10.40	0.006 ± 0.035
<i>NGC</i> 4665	0.0	3.80	785	0.83	8.2	7.57	0.008 ± 0.035
<i>NGC</i> 4670	0.0	1.44	1112	0.76	7.5	5.61	0.348 ± 0.052
<i>NGC</i> 4691	0.0	2.82	1108	0.81	13.1	4.74	0.448 ± 0.057
<i>NGC</i> 4763	1.0	1.51	4160	0.71	8.4	4.14	0.091 ± 0.050
<i>NGC</i> 4765 ^c	0.0	1.06	706	0.72	5.0	5.09	0.120 ± 0.026
<i>NGC</i> 4778	−1.0	0.71	4355	0.67	4.9	2.55	0.008 ± 0.037
<i>NGC</i> 4795	0.5	1.86	2684	0.85	18.8	2.73	0.254 ± 0.104
<i>NGC</i> 5548 ^c	0.0	1.16	5026	0.89	9.0	3.25	0.192 ± 0.050
<i>NGC</i> 5614	2.0	2.45	3872	0.83	10.1	3.93	0.117 ± 0.096
<i>NGC</i> 5691	1.0	1.86	1846	0.76	9.8	5.23	0.357 ± 0.139
<i>NGC</i> 5695	0.0	1.55	4206	0.71	9.4	2.51	0.109 ± 0.044
<i>NGC</i> 5701 ^c	0.0	1.63	1556	0.95	11.0	4.22	0.012 ± 0.025
<i>NGC</i> 5915	2.0	1.74	2245	0.72	5.0	3.48	0.204 ± 0.109
<i>NGC</i> 5963	0.0	3.31	770	0.77	7.8	5.40	0.076 ± 0.065
<i>NGC</i> 6012	2.0	2.09	1988	0.72	11.4	3.70	0.032 ± 0.042
<i>NGC</i> 6646	1.0	1.23	5764	0.85	7.4	4.43	0.012 ± 0.038
<i>NGC</i> 6962	2.0	2.88	4254	0.79	10.4	3.69	0.053 ± 0.037

^athe diameter of the galaxy out to the isophote of surface brightness 25 mag/arcsec²

^bthe ratio of the minor to major axis as defined in the RC3 catalogue

^cThe last three columns are the averages for multiple images

Table 2. Characteristics of Multicolor Sample

object name	T	D ₂₅ ^a [']	v _{rec} [km/s]	b/a ^b
<i>IC</i> 1269	4.0	1.70	6116	.74
<i>NGC</i> 5600	5.0	1.44	2319	.95
<i>NGC</i> 6555	5.0	2.00	2225	.78

^athe diameter of the galaxy out to the isophote of surface brightness 25 mag/arcsec²

^bthe ratio of the minor to major axis as defined in the RC3 catalogue

REFERENCES

- Baldwin, J.E., Lynden-Bell, D., Sancisi, R. 1980, MNRAS, 193, 313
- Barnes, Joshua E., Hernquist, Lars, 1992, ARA&A, 30, 705
- Byun, Y. I., Freeman, K. C., Kylafis, N. D. 1994, ApJ, 432, 114
- Carlberg, R. G. 1990, ApJ, 359, L1
- Charlot, S., Bruzwal, G. A. 1991, ApJ, 367, 126
- Conselice, C. J. 1997, PASP, In Press
- De Vaucouleurs, G. 1991, Third Reference Catalogue of Bright Galaxies
(New York : Springer Verlag)
- Hernquist, Lars, Mihos, Christopher 1995. ApJ, 448, 41
- Kennicutt, R. C. 1992, ApJ, 388, 310
- Kennicutt, R. C. 1992, ApJS, 79, 255
- Kennicutt, R. C., Tamblyn, P., Congdon, C.W. 1994, ApJ, 435, 22
- Lacey, C., Cole, S. 1993, MNRAS, 262, 627
- Levine, Stephen E., Sparke, Linda S. 1998, ApJ, 496, L13
- Mihos, Christopher, Hernquist, Lars 1994, ApJ, 425, 13
- Richter, O.-G., Sancisi, R. 1994, A&A, 290, L9
- Rix, H.-W., Zaritsky, D. 1995, ApJ, 447, 82
- Sellwood, J. A. 1985, MNRAS, 217, 127
- Sellwood, J. A., Merritt, David 1994, ApJ, 425, 530
- Syer, D., Tremaine, S. 1996, MNRAS, 281, 925
- Tóth, G., Ostriker, J. P. 1992, ApJ, 389, 5
- Walker, I. R., Mihos, C., Hernquist, L. 1996, ApJ, 460, 121
- Zang, T. A., Hohl, F. 1978, ApJ, 226, 521

Zaritsky, D., Rix, H.-W. 1997, ApJ, 477, 118

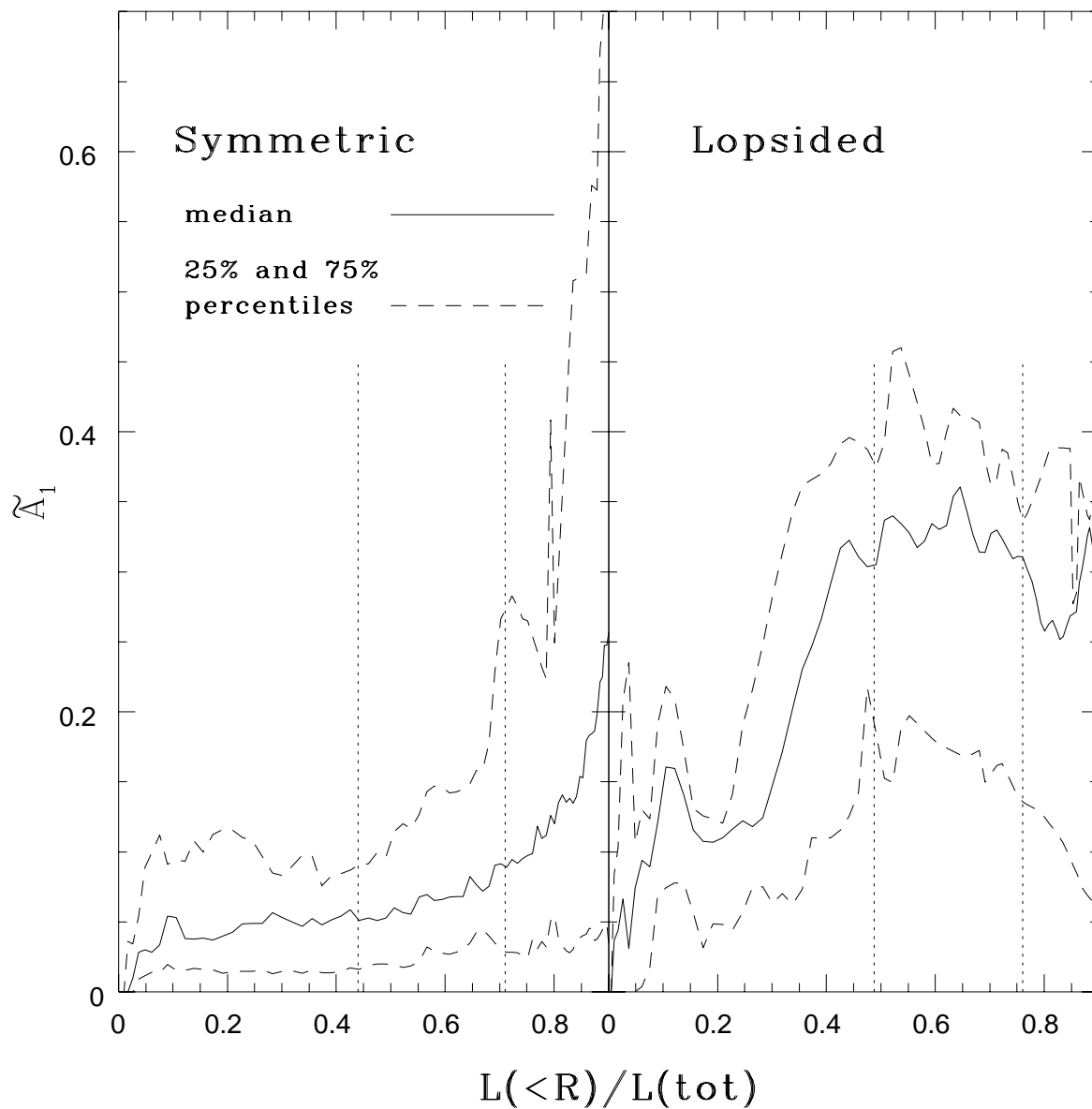


Fig. 1.— The median $\tilde{A}_1(L(\leq R)/L(\text{tot}))$ profiles for the 20% most lopsided galaxies in our sample and the 80% least lopsided for whom $L(\leq R)/L(\text{tot}) \geq 0.71$ ($R_{\text{max}} \geq 2.5R_{\text{exp}}$). The dotted lines contain the central 50% of the points. The vertical dotted lines indicate the radial range over which $\langle \tilde{A}_1 \rangle$ was determined.

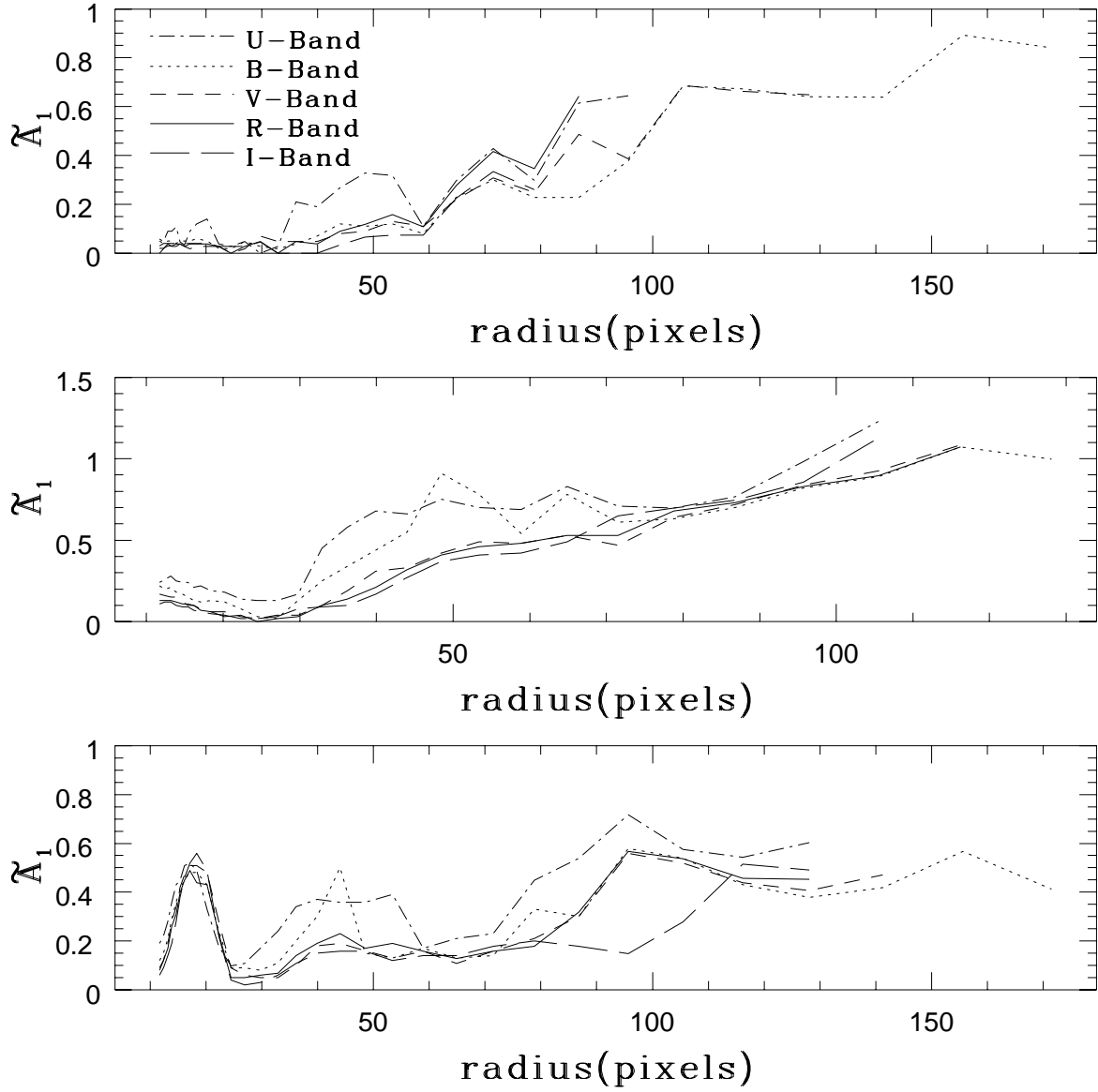


Fig. 2.— The UBVRI $\tilde{A}_1(R)$ profiles for three late type spiral galaxies: IC 1269 (top), NGC 5600 (middle) and NGC 6555 (top). U and B-band images exhibit deviations from the mean profile, but V,R and I-band images are generally congruent.

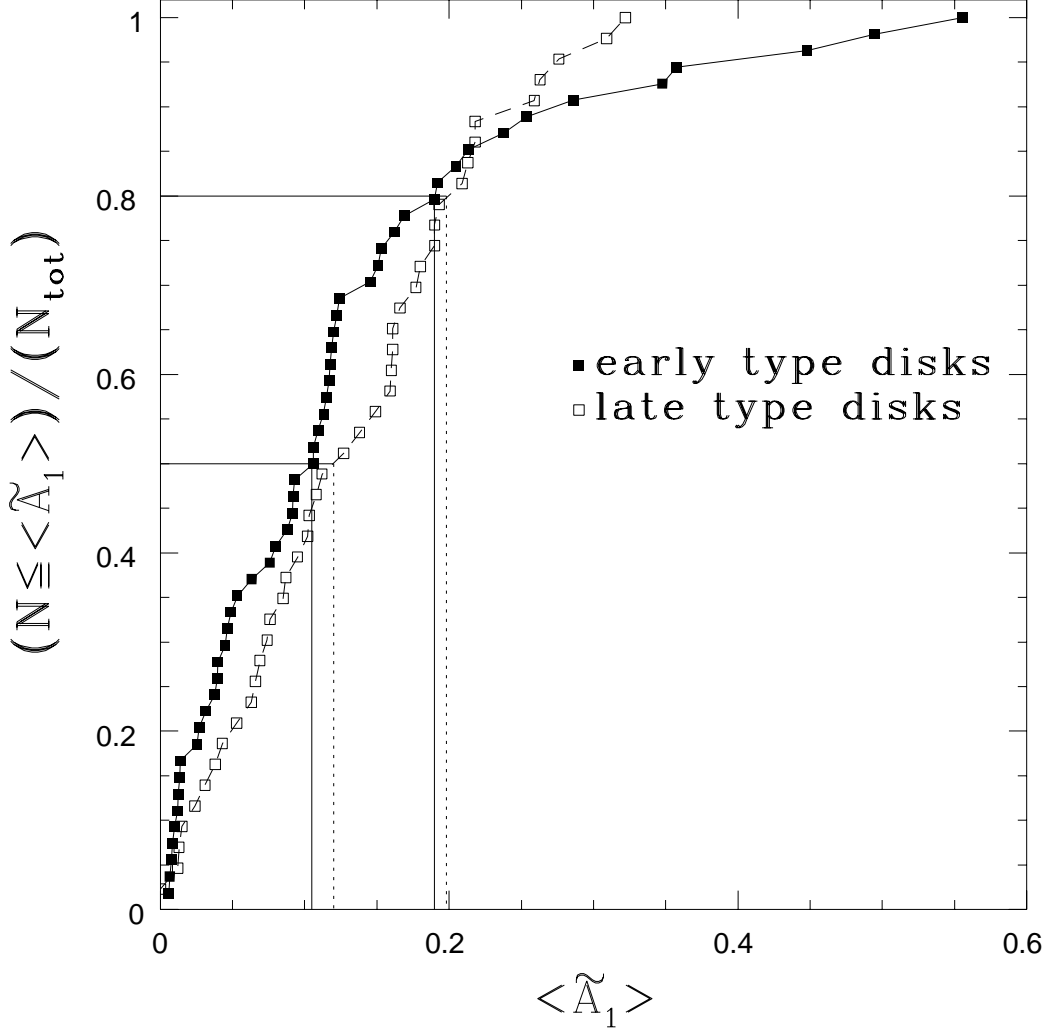


Fig. 3.— The cumulative histograms of $\langle \tilde{A}_1 \rangle$ for the current sample and for the sample of ZR97. The very small differences between $\langle A_1 \rangle$ and $\langle \tilde{A}_1 \rangle$ in ZR97 do not affect our comparison of the two samples. The y-axis is the fraction of galaxies in the sample with $\langle \tilde{A}_1 \rangle \leq$ a certain amount. There are 43 Late Type disk and 54 early type disk galaxies. Note that the current sample has 3 galaxies with significantly higher $\langle \tilde{A}_1 \rangle$ than ZR97. We account for the ZR97 star subtraction methods by subtracting the offset (0.03) from all of their data points.